


# Tunable acoustic transmission control and dual-mode ventilated sound insulation by a coupled acoustic metasurface

Siyuan Gao<sup>✉</sup>, Xinghao Hu, Youyu Mo, Haohan Zeng, Feilong Mao, Yifan Zhu<sup>✉,\*</sup>, and Hui Zhang<sup>✉,†</sup>  
*Jiangsu Key Laboratory for Design and Manufacture of Micro-Nano Biomedical Instruments, School of Mechanical Engineering, Southeast University, Nanjing 211189, China*

 (Received 7 March 2024; revised 4 April 2024; accepted 5 April 2024; published 24 April 2024)

In this paper, we present an alternative design for an acoustic metasurface with sparse units featuring open-ended pipes located on both sides of a central cavity, which can be tuned by designing the widths and length sizes. Band-stop and band-pass transmission control can be easily attained by alternating these units' periodic arrangements with and without intervals and can be theoretically computed by the transfer-matrix method. By combining four of these units, the formed coupled metasurface has a subwavelength of  $0.127\lambda$  and can insulate broadband sound (4.2 cm for approximately 1000–1500 Hz). The working bandwidth is between the resonant frequencies of monopolar and dipolar modes, which correspond to a negative effective bulk modulus and a negative effective-mass density, respectively, whose mechanism is different from conventional ones. To help with the tuning, the acoustic-electrical analogy gives the operating frequency as a function of size parameters. Numerical simulations and experiments are used to verify the ventilated sound insulation and transmission control capabilities. This paper presents a structurally simple, lightweight, and multifunctional design with appropriate arrangements that can be applied to acoustic communications, architectural acoustics, noise control, and other related fields.

DOI: [10.1103/PhysRevApplied.21.044045](https://doi.org/10.1103/PhysRevApplied.21.044045)

## I. INTRODUCTION

Acoustic metamaterial [1] and acoustic metasurfaces [2] have drawn a lot of attention from researchers over the last two decades because of their unique properties—like negative bulk modulus [3,4] and negative mass density [5]—that do not exist in natural materials and could offer an incredibly thin solution for real-world acoustic issues.

Extensively researched and intricately designed metamaterials or metasurfaces enable the realization of a multitude of unusual acoustic transmission controls, including refraction [6,7], extraordinary transmission [8], cross-media transmission enhancement [9,10], transmitted amplitude or phase manipulation [11–13], and wave-front transformation [14]. On the very opposite of sound transmission, acoustic trapping [15], absorption, and reflection are required in cases like energy harvesting [16] and noise reduction [17–19]. Coiled or cascaded metamaterials [20,21], Fabry-Pérot tubes [22,23], Helmholtz resonators [24–26], Mie resonators [27,28], and sparse structures with Fano interferences [29–31] are studied and developed to assist noise control by sound absorption or sound insulation, most of which are simultaneously able to allow airflow [20,21,23–29,31]. However, because of the intricate arrangements along the sound path (such as

gradient unit cells), conventional broadband ventilated noise reduction metastructures typically have a significant thickness [24,25,32–34], which restricts their applicability.

In this paper, we propose an alternative mechanism whereby the obtained broadband bandwidth depends on the coupling of two resonant modes of the unit cell, rather than on gradient arrangements. It is interesting to note that the resonant frequencies of the monopolar and dipolar modes, respectively, correspond to the lower and upper frequencies of the sound-insulation bandwidth. Negative effective-mass density and negative effective bulk modulus can be reached at the dipolar and monopolar modes, respectively.

To prove this mechanism, we study the metasurface from the initial unit design to the four-unit coupled structures. Specifically, a sparse unit featuring open-ended tubes located on both sides of a central cavity is designed. By simply altering the periodical arrangement of the units without intervals and with intervals, acoustic control of extraordinary sound transmission and sound insulation at the same frequency range (narrow band) can be realized. This design is also proved readily tunable by giving a theoretical operating frequency as a function of size parameters including tubes' widths and unit lengths. Later, we broaden the working frequency range by coupling four units and inspiring two working modes (monopole and dipole) and achieve a tunable broadband ventilated sound insulation with a structure thickness down to  $0.127\lambda$ , showing the

\*Corresponding author: [yifanzhu@seu.edu.cn](mailto:yifanzhu@seu.edu.cn)

†Corresponding author: [seuzhanghui@seu.edu.cn](mailto:seuzhanghui@seu.edu.cn)

advantage of this mechanism. This multifunctional unit design and coupled design might offer another approach to acoustic transmission manipulation and noise-control problems.

## II. UNIT DESIGN AND TRANSMISSION CONTROL

Enlightened by the Helmholtz resonator and folded Fabry-Pérot tubes, a composite unit consisting of a cavity and tubes is designed. The overall shape of the designed unit is a rectangular cuboid with dimensions of  $L \times L \times H$ . When altering the design, it should be noted that to prevent higher-order waveguide modes, the height should be less than  $\lambda/2$ , where  $\lambda$  is the wavelength corresponding to the working frequency. The left part of Fig. 1(a) displays its cross-section schematic, which includes two narrower pipes of different widths on both sides and a wider cavity in the center, forming a folded sound-transmission path. The incident sound wave propagates along the positive  $y$ -axis direction. The sizes of the two narrower pipes are determined by  $W_1$  and  $W_2$ , and their widths are  $w_1 = L - W_1 - t$  and  $w_2 = L - W_2 - t$ , respectively, in which  $t$  is the wall thickness of the unit. The width of the internal cavity can also be fixed by the above parameters. The relationship between the working frequency and the parameters  $L$ ,  $W_1$ , and  $W_2$  of each unit will be introduced later to illustrate the tuning feasibility of this unit structure.

Arranging the above units periodically with intervals and without intervals, two different metasurfaces of opposite sound-transmission properties can be formed. When the interval exists, and the width of the ventilated gap is  $D = 50$  mm, as shown in the upper right part of Fig. 1(a), ventilation and sound insulation can be simultaneously achieved within the working frequency range. Whereas the interval is canceled ( $D = 0$  mm), as shown in the bottom right part of Fig. 1(a), the metasurface is capable of transmitting sound power effectively within the working frequency range instead. The dynamic adjustment of the intervals can be realized by connecting the units with springs or scissor mechanisms.

This peculiar band-pass and ventilated band-stop effect stems from the transmission characteristics of the unit. The transmittance spectrum of a specific unit is calculated by applying the transfer matrix method [11,35] and verified through numerical simulation with COMSOL Multiphysics 6.0 and the experiment in the impedance tube. Sec. S1 within the Supplemental Material contains the detailed work of the analytical transmission coefficient of the unit and Sec. S2 within the Supplemental Material contains the experimental evidence [36]. The results given by the transmittance spectrum is that at the resonant frequency, the phase jumps by  $180^\circ$ , outputting an inverted acoustic wave with a near-unity transmittance. This transmitted wave results in the band-pass effect itself or interferes with

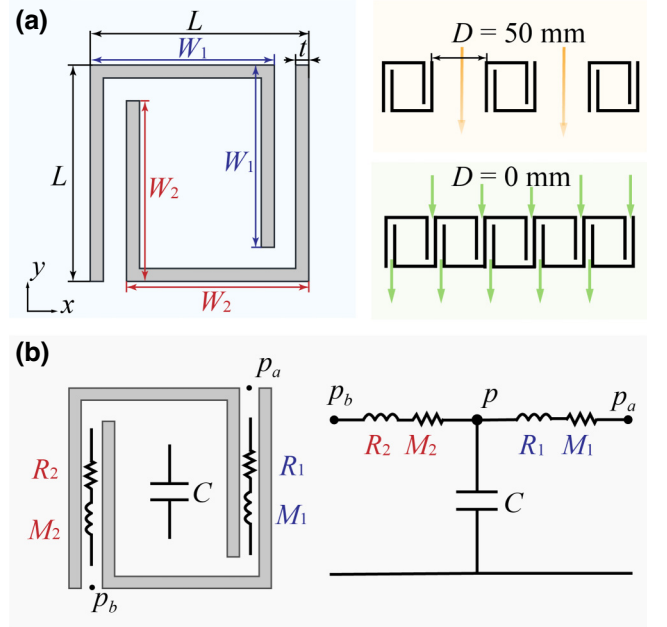


FIG. 1. (a) Schematic of the single unit and arrangements of these units to form the two metasurfaces; (b) schematic of applying acoustic-electrical analogy to a unit and its equivalent electrical circuit.

the forward acoustic wave propagating at the ventilated gap (the interval of the units), leading to the ventilated band-stop effect.

The resonant frequency of a unit can be derived by the acoustic-electrical analogy [37]. This method offers a theoretical formula for the tunable properties of the unit by presenting the relationship between the resonant frequency and the unit dimensions. As shown in Fig. 1(b), the narrow tubes on both sides can be considered as a series connection of the resistance

$$R_x = \frac{\sqrt{2}\mu_0\rho_0\omega L_x}{w_x S_x} (x = 1, 2)$$

and the inductance

$$M_x = \frac{\rho_0 L_{\text{eff}_x}}{S_x} (x = 1, 2),$$

where the dynamic viscosity of air  $\mu_0 = 1.86 \times 10^{-5}$  Pa s, air density  $\rho_0 = 1.21$  kg/m<sup>3</sup>, the effective tube length is given by  $L_{\text{eff}_x} = \sqrt{w_x^2 + (L - t)^2}$  ( $x = 1, 2$ ) and the tube cross-section area  $S_x = w_x H$  ( $x = 1, 2$ ). The middle cavity can be analogized to a capacitor whose value is  $C = V_0 / \rho_0 c_0^2$ , where the cavity volume  $V_0 = (W_1 + W_2 - L)HL$  and the speed of sound in air  $c_0 = 343$  m/s.

By applying Kirchhoff's current law at the node of the sound pressure in the cavity, the operating frequency of the

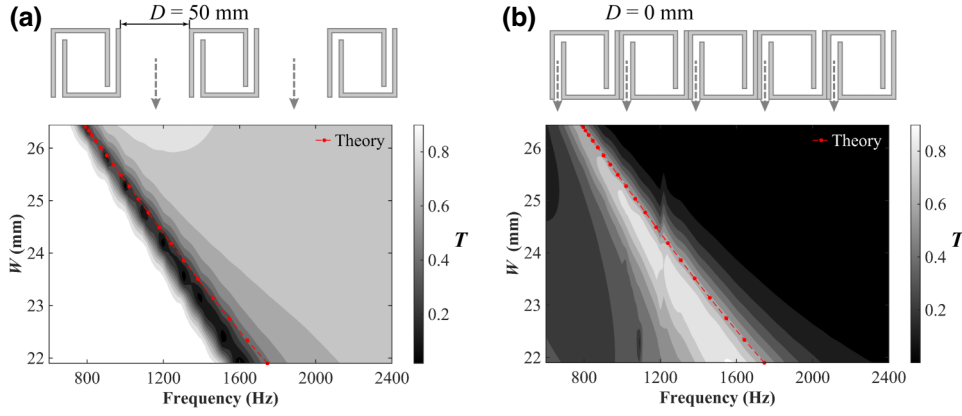


FIG. 2. (a) Dependence of the transmittance of the sound-insulation metasurface ( $D = 50$  mm,  $t = 1.5$  mm, and  $L = 30$  mm) on the width parameters and frequency from the results of simulation and a line plotted according to the theoretical model. (b) Dependence of the transmittance of the sound-transmission metasurface ( $D = 0$  mm,  $t = 1.5$  mm, and  $L = 30$  mm) on the width parameters and frequency from the results of simulation and a line plotted according to the theoretical model.

unit can be derived as [32]

$$f_d = \frac{1}{2\pi} \left( \frac{\mu_0}{\rho_0 w_1 w_2} + \frac{1}{2} \sqrt{\left( \frac{2\mu_0}{\rho_0 w_1 w_2} \right)^2 + \frac{4B(A_1 + A_2)}{A_1 A_2}} \right), \quad (1)$$

where

$$A_x = \frac{\sqrt{w_x^2 + (L - t)^2}}{w_x} \quad (x = 1, 2)$$

and

$$B = \frac{c_0^2}{(W_1 + W_2 - L)L}.$$

It should be noted that the term  $\mu_0/\rho_0 w_1 w_2$  in Eq. (1) represents the thermal viscous effect in the narrow tubes; however, it is negligible compared to the term  $\sqrt{4B(A_1 + A_2)}/A_1 A_2$  when it comes to the calculation of resonant frequency. Therefore, Eq. (1) can be simplified as follows:

$$f_d = \frac{1}{2\pi} \sqrt{\frac{B(A_1 + A_2)}{A_1 A_2}}. \quad (2)$$

From Eq. (2), it can be seen that the operating frequency depends only on the size parameters  $L$ ,  $W_1$ , and  $W_2$ , implying that the unit is capable of easy tuning by designing the function  $f_d(W_1, W_2, L)$ .

To validate the theory and assess the sound block or sound-transmission effect, two designed metasurfaces are numerically simulated using the ‘‘Pressure Acoustics Module’’ of the commercial simulation software COMSOL Multiphysics 6.0. The ‘‘Thermoviscous Acoustics Module’’ is introduced into the unit cell, and the wall surface of the structure is configured as an acoustic hard boundary, while

the incident and outgoing ends are set as plane-wave radiation conditions, and the lateral sides are set as periodic boundary conditions. The simulation is carried out for the frequency range of 600 to 2400 Hz.

By fixing  $L = 30$  mm and altering the values of  $W_1$  and  $W_2$ , numerical simulation is performed to verify Eq. (2) and demonstrate the transmission control of band pass and band stop. The transmission spectrum of the sound-insulation metasurface with a unit interval of 50 mm is shown in Fig. 2(a), where darker colors indicate smaller transmission coefficients and whiter colors indicate larger ones. Intuitively, the metasurface exhibits soundproof properties near the operating frequency, and as  $W_1$  and  $W_2$  increase (i.e., the sizes of the two narrow tubes decrease and the middle cavity increases), the operating frequency tends to be lower, but the bandwidth becomes narrower. On the other hand, Fig. 2(b) depicts the transmission spectrum of the sound-transmission metasurface with a unit spacing of 0 mm, revealing a high transmission of sound intensity near the operating frequency. As the operating frequency decreases, the bandwidth also becomes narrower, and the transmission effect was marginally worse at low frequencies because of a more significant thermal viscous effect of the narrow tubes. The simulation results closely matched the theoretical curve, demonstrating that by varying the  $W_1$  and  $W_2$  of the unit cell, the operating frequency of the metasurface can be effectively tuned. Additionally, by adding or canceling the unit spacing  $D$ , pass-band and stop-band effects could be achieved, respectively.

### III. FOUR-UNIT COUPLED METASURFACE

Ventilated sound insulation in practical applications normally necessitates a structure operating at a wider frequency band than at a single frequency. It is natural to think of connecting units of different operating frequencies

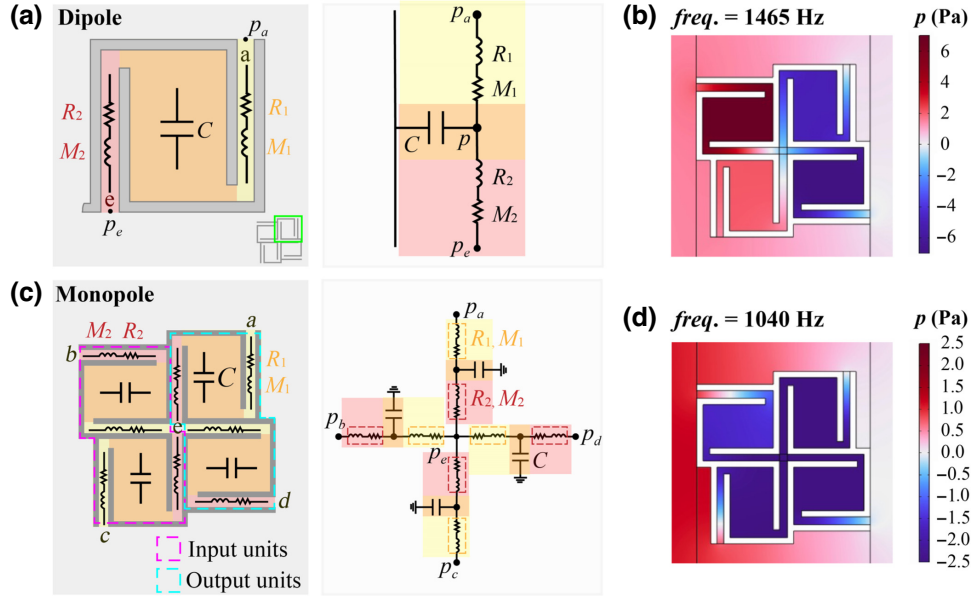


FIG. 3. (a) The equivalent circuit of dipolar working mode. (b) The sound-pressure field distribution of sample  $A$  ( $L = 20$  mm,  $W_1 = 16.6$  mm,  $W_2 = 16.89$  mm, and  $t = 1.5$  mm) working at the dipolar frequency (1465 Hz). (c) The schematic of the four-unit coupled cell and the equivalent circuit of monopolar working mode. (d) The sound-pressure field distribution of sample  $A$  working at the monopolar frequency (1040 Hz).

in series, which is our prior research [32], and it has an obvious shortcoming of a relatively large sample length.

To increase the frequency range of sound insulation with a smaller sample size, the single-unit designs can be combined in the form shown in Fig. 3(c) by joining the four tubes in the center. Now, we define the single unit as a unit and the whole coupled four-unit structure as a cell. We may name the four units by connecting the letters labeled at the input and output tubes; for instance, the upper left cell is identified as “ $be$ ” and the upper right cell is labeled as “ $ea$ .” The “ $be$ ” and the “ $ce$ ” units are input units where the external sound enters the cell from the front and the ventilated gap, respectively, whereas the “ $ea$ ” and the “ $ed$ ” units are output units. The combination gives rise to two acoustic modes: the dipole and the monopole. The acoustic-electrical analogy will be used to discuss the resonant frequencies and sound-pressure characteristics of these modes in the following.

The dipolar working mode can be viewed as each unit performing separately, with zero sound pressure in the center, namely  $p_e = 0$  as shown in Fig. 3(a). Therefore, dipolar frequency shares a similar calculation method as the unit’s resonant frequency discussed before, which follows Eq. (2). In Fig. 3(b), it can be observed that the sound pressure in the output units is out of phase with the input units and the ventilated gap. Exactly like the unit function we have introduced before, the interference between the resonance in the cell and the continuum state in the gap, or Fano-like interference, imparts the possibility of ventilated acoustic insulation in this artificial metasurface.

The monopolar working mode is a coupled acoustic mode established by the combination of the four units, permitting sound insulation at a lower frequency. The equivalent circuit applying the acoustic-electrical analogy is illustrated in Fig. 3(c). In this case, the sound pressure in the center of the combined cell is the maximum value. Similar to Eq. (1), by applying Kirchhoff’s current law at the node of the sound pressure in the geometry center of the four-unit cell, namely  $p_e$ , by grounding  $p_a, p_b, p_c$ , and  $p_d$  and neglecting the resistance, the following equation can be written:

$$\frac{2p_e}{1/(j\omega C + 1/j\omega M_2) + j\omega M_1} + \frac{2p_e}{1/(j\omega C + 1/j\omega M_1) + j\omega M_2} = 0. \quad (3)$$

The solution to Eq. (3) and the monopolar frequency is as follows:

$$f_m = \frac{1}{2\pi} \sqrt{\frac{B(2 + \sqrt{2 - A_2/A_1 - A_1/A_2})}{A_1 + A_2}}, \quad (4)$$

where  $A_x$  ( $x = 1, 2$ ) and  $B$  are of the same form as in Eq. (2).

The acoustic phase inside the cell’s units, as shown in Fig. 3(d), is in-phase, whereas in the output tubes of unit “ $ea$ ” and unit “ $ed$ ,” the acoustic phase is opposite to that in the gap, offering the premise for sound attenuation through interference.



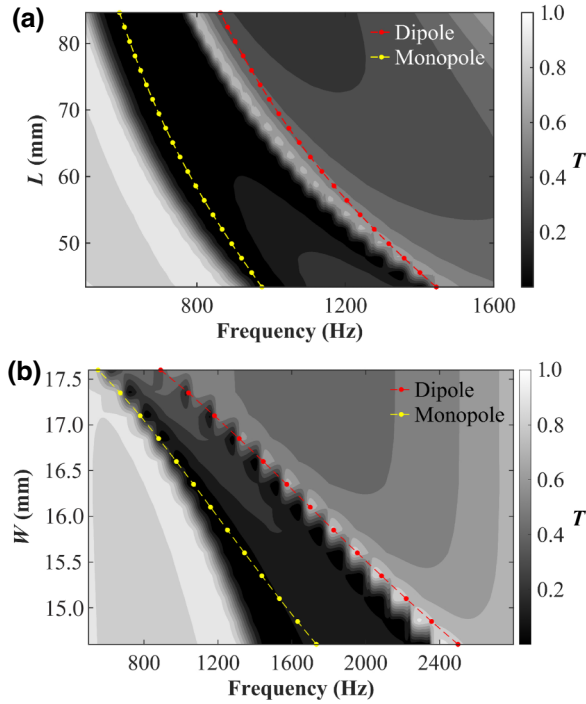


FIG. 4. (a) Dependence of the transmittance of the four-unit coupled metasurface ( $D = 50$  mm,  $t = 1.5$  mm,  $W_1/L = 0.83$ , and  $W_2/L = 0.8445$ ) on the unit-length parameter  $L$  and frequency from the results of simulation and two lines plotted at the dipolar and monopolar frequencies according to the theoretical model. (b) Dependence of the transmittance of the four-unit coupled metasurface ( $D = 50$  mm,  $t = 1.5$  mm, and  $L = 20$  mm) on the width parameter  $W$  and frequency from the results of simulation and two lines plotted at the dipolar and monopolar frequencies according to the theoretical model.

By combining the four units, the newborn coupled cell is granted a lower-frequency mode of monopole and inherits a higher-frequency mode of the dipole, all these modes offering an opposite output phase with the ventilated gap and causing the aforementioned Fano-like interference to achieve sound insulation. The theoretical formulas and analogies are validated through numerical simulations, which also demonstrate the four-unit coupled metasurface's tunability.

To confirm the theoretical modes and further expound the broadband and tunable feature of the designed metasurface, we numerically calculate the parameter dependences of transmission spectrum on the unit length  $L$  by fixing the ratio of  $W_x$  ( $x = 1, 2$ ) and  $L$ , whose results are shown in Fig. 4(a), and on the unit widths  $W$  by fixing the length  $L$ , whose results are illustrated in Fig. 4(b). The dipolar and monopolar frequencies from the theoretical model are also plotted in Figs. 4(a) and 4(b), which approximately fit the boundaries of the sound insulation band (dark-colored area), and the cause of the discrepancy might be that when  $W$  is too small, the original assumptions of the

two tubes and center cavity in acoustic-electrical analogy might fail. The two figures demonstrate unambiguously that the two monopolar and dipolar modes are responsible for the lower and the higher resonant frequencies, respectively, and between these modes, the transmittance is also small enough for sound insulation, indicating a much more broadband performance, which is about 1000 Hz, compared to the spectrum shown in Fig. 2(a). As for the tuning ability, the working frequency range can be adjusted to a lower-frequency region by either increasing the unit length or increasing the ratio of  $W/L$ , though a high ratio may lead to a smaller frequency band and a poorer effect, possibly since the increasing thermal viscous effect in the thinner tubes reduces the transmitted output of the cell and thereby weakens the interference, albeit the slightly improved sound absorption.

#### IV. EFFECTIVE MEDIUM DESCRIPTION

The effective medium theory [38] is the method that converts a complex structure into an effective medium by taking into account its effective parameters like density and bulk modulus. Applying the standard procedure [38–40], which is thoroughly explained in Sec. S3 within the Supplemental Material [36], will yield these effective parameters.

Two samples, one designed for a lower frequency (sample *A*), and another for a higher one (sample *B*), are numerically tested to reveal the sound insulation performance. Sample *A*'s specific size parameters are as follows: unit length  $L = 20$  mm, wall thickness  $t = 1.5$  mm, unit width parameters  $W_1 = 16.6$  mm,  $W_2 = 16.83$  mm, and the distance between cells (width of ventilated gap)  $D = 25$  mm. The only difference between sample *A* and sample *B* is the width parameters, in which sample *B*'s widths are  $W_1 = 14.6$  mm, and  $W_2 = 14.89$  mm. This alternation directly tunes the working frequency range, proving the high tuning ability of cell design.

Figure 5 shows the spectrum of the two samples' sound-transmission performances and their effective parameters. We may take sample *B*, for example, to describe the relationship between the two modes and the negative effective parameters. From Figs. 5(c) and 5(d), it can be found that the monopolar mode, working at around 1500 Hz, offers a close-to-zero transmittance, and accordingly, the structure exhibits a negative bulk modulus at the frequency range of 1405–1695 Hz. Meanwhile, the dipolar mode corresponds to a negative mass density at a stop-band frequency range of 2220–2435 Hz, also giving a low sound transmission. The results of lower-frequency sample *A*, shown in Figs. 5(a) and 5(b) are fairly similar, which can be concluded as two different modes corresponding to two negative parameters and the coupled effects of both modes leading to a low transmittance between the two mode frequencies. The lower-frequency sample *A* has narrower side tubes, leading

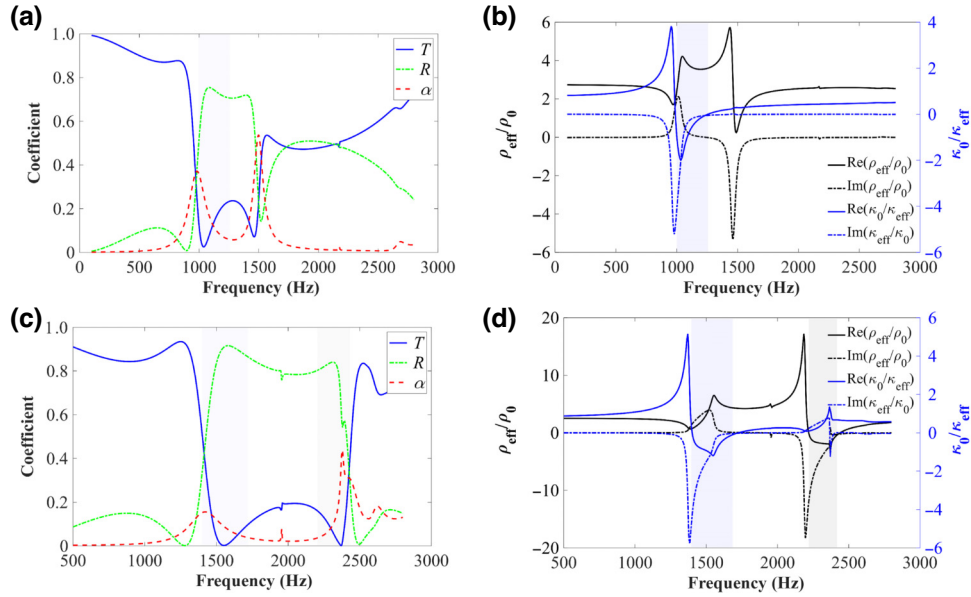


FIG. 5. (a) Sample *A*'s spectrum of the transmittance  $T$ , the reflectance  $R$ , and the sound-absorption coefficient  $\alpha$ . (b) The effective medium description of sample *A* (shaded area as the interval of the negative effective parameter), where  $\rho_{\text{eff}}$  is the effective mass density and  $\kappa_{\text{eff}}$  is the effective bulk modulus. (c) Sample *B*'s spectrum of the transmittance  $T$ , the reflectance  $R$ , and the sound absorption coefficient  $\alpha$ . (d) The effective medium description of sample *B* (shaded areas as the intervals of the negative effective parameters).

to a stronger thermal viscous effect and a higher absorption coefficient ( $\alpha = 1 - T - R$ ) at resonant frequencies, but suffering from a weakened interference and a poorer sound-insulation performance. A comparative simulation without considering the thermal viscous effect is conducted and results are analyzed in Sec. S4 within the Supplemental Material [36].

Samples *A* and *B* are tuned by altering the parameter  $W$  when fixing the length  $L$ . With a limited overall size, the ratio  $W/L$  gets much too high for low-frequency sound insulation, which results in the aforementioned weakened interference. Another sample *C* is designed by fixing the ratio  $W/L$  as the same as sample *B* and properly enlarging the overall size (changing parameter  $L$ ), and the details and its low-frequency working performance are recorded in Sec. S5 within the Supplemental Material [36]. These two samples both have a thickness of less than 44 mm, which is down to  $0.127\lambda$  (subwavelength), and they give a relatively broadband sound insulation. By following this principle of design (designing  $f_d(W_1, W_2, L)$  and  $f_m(W_1, W_2, L)$ ), and connecting different samples in series, noise at the intended frequency range can be suppressed effectively.

## V. EXPERIMENTAL EVIDENCE

We fabricated the two four-unit coupled samples (sample *A* and sample *B*) with height parameter  $H = 25$  mm, whose photo is shown in Fig. 6(a), and inserted them individually into the parallel plate experimental system, whose schematic is shown in Fig. 6(b). The system consists

of two thick acrylic panels between which the sample is placed, the speaker, microphones at the measuring areas, and the sound-absorbing cotton stuffed around the panels. The loudspeaker was placed half a meter away from the entrance of the tested sample to be equivalent to plane-wave incidence (see Sec. S6 within the Supplemental Material [36]) and the input signal utilized is the sine-sweep signal ranging from 400 to 4000 Hz. Two sets of data were collected with and without the sample, where the incident sound waves were measured at the incident measuring area without the sample to avoid the interference of the reflected waves. The transmittance spectrums by experiment and by simulation are plotted in Fig. 6(d) for sample *A* and Fig. 6(e) for sample *B*. The experiment results show effective sound insulation at the frequency range from approximately 990 to 1450 Hz for sample *A* and from 1455 to 2430 Hz for sample *B*. The two modes, monopole and dipole, are reflected clearly in the experiment curves, well fitting the simulation curves.

After testing the two samples separately, we combine these two samples in the form of a series connection [the connection method shown in Fig. 6(f) with a distance between two samples  $d_s = 40$  mm] to demonstrate multiple layers of the designed metasurface are capable of broadband sound insulation. Figure 6(f) also shows the two-layer structure's sound transmission loss (STL), which is calculated by  $\text{STL} = 10 \lg 1/T$ , where  $T$  is the transmittance, indicating an over 15 dB average STL from approximately 1030 to 2425 Hz. The monopole and dipole of sample *A* and the dipole of sample *B* can be recognized

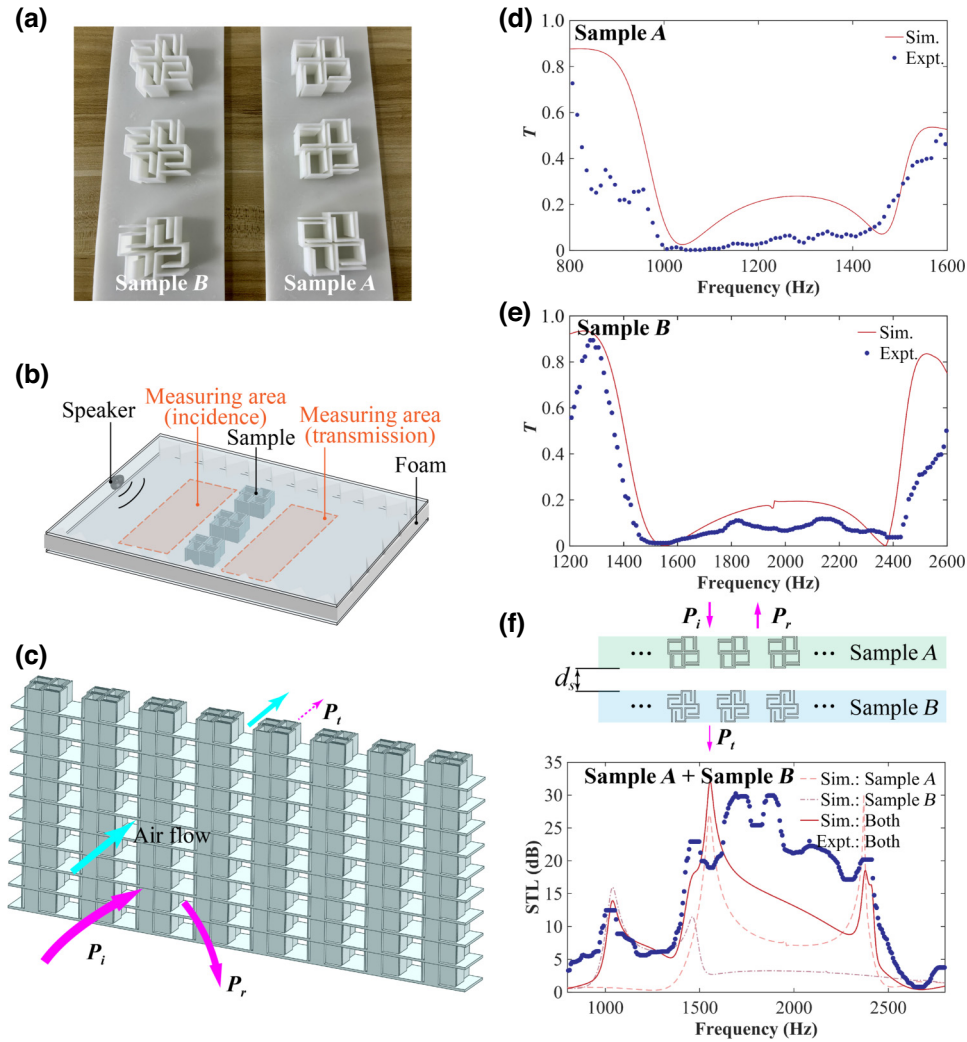


FIG. 6. (a) The photo of sample *A* and sample *B* fabricated by three-dimensional printing. (b) Schematic of the parallel-plate experimental system. (c) Schematic of an acoustic barrier formed by the four-unit coupled metasurface. (d) Simulated and experimental results of sample *A*'s transmission spectrum. (e) Simulated and experimental results of sample *B*'s transmission spectrum. (f) Schematic of the series connection of two samples and the connection's simulated and experimental results of the sound-transmission loss.

in the experimental curve with clear STL peaks. The discrepancies between the simulation and experiment may be due to the fabrication error and the possible reflection caused by the poor acoustic absorption of the surrounding acoustic foam.

An example of a potential structure for a sound-insulation barrier that could be created by piling up the designed coupled four-unit metasurface is shown in Fig. 6(c). This type of barrier could be used in ventilated cases for sound-insulation purposes, such as industrial noise control and architectural acoustics.

## VI. CONCLUSION

We have designed an acoustic unit consisting of two tubes and a middle cavity. By applying acoustic-electrical analogy and transfer-matrix method, the relationship

between the resonant frequency and the dimensional parameters  $W_1$ ,  $W_2$ , and  $L$  is given to instruct the tuning of the structure. The function of this unit can be changed by different arrangements. Metasurfaces with the combination of units with and without intervals exhibit opposite transmission characteristics, which are stop band and pass band, respectively. The pass-band effect is numerically and experimentally verified and fits well with the theoretical model. We also introduce a four-unit coupled metasurface, which inherits the dipolar mode and derives a monopolar mode, developing a relatively broadband sound insulation with an interesting dual-mode coupling mechanism. The effective medium theory and acoustic-electrical analogy are used to describe the two resonant modes and estimate their resonant frequencies. The estimation is verified by numerical simulation and the experiment with two samples, featuring a working frequency range from 1040–1465

and 1526–2365 Hz with a thickness of approximately  $0.127\lambda$ . The designs are endowed with a subwavelength thickness, sound-transmission control (narrowband ventilated band stop and band pass, and broadband ventilated insulation), the possible band widening by a combination of multiple layers, and the ability to tune the operating frequency, giving a possibility of multiple practical application scenarios, such as ventilated acoustic insulation and acoustic communications.

### ACKNOWLEDGMENTS

This work was supported by the National Natural Science Foundation of China (Grant No. 52272433); the Natural Science Foundation of Jiangsu Province (Grant No. BK20220798); and the Young Elite Scientists Sponsorship Program by JSAST (Grant No. TJ-2022-012).

- 
- [1] G. Ma and P. Sheng, Acoustic metamaterials: From local resonances to broad horizons, *Sci. Adv.* **2**, e1501595 (2016).
- [2] B. Assouar, B. Liang, Y. Wu, Y. Li, J.-C. Cheng, and Y. Jing, Acoustic metasurfaces, *Nat. Rev. Mater.* **3**, 460 (2018).
- [3] Z. Liu, X. Zhang, Y. Mao, Y. Y. Zhu, Z. Yang, C. T. Chan, and P. Sheng, Locally resonant sonic materials, *Science* **289**, 1734 (2000).
- [4] N. Fang, D. Xi, J. Xu, M. Ambati, W. Srituravanich, C. Sun, and X. Zhang, Ultrasonic metamaterials with negative modulus, *Nat. Mater.* **5**, 452 (2006).
- [5] Z. Yang, J. Mei, M. Yang, N. H. Chan, and P. Sheng, Membrane-type acoustic metamaterial with negative dynamic mass, *Phys. Rev. Lett.* **101**, 204301 (2008).
- [6] Z. Liang and J. Li, Extreme acoustic metamaterial by coiling up space, *Phys. Rev. Lett.* **108**, 114301 (2012).
- [7] Z. Hou, X. Fang, Y. Li, and B. Assouar, Highly efficient acoustic metagrating with strongly coupled surface grooves, *Phys. Rev. Appl.* **12**, 034021 (2019).
- [8] Y. Li, B. Liang, X. Zou, and J. Cheng, Extraordinary acoustic transmission through ultrathin acoustic metamaterials by coiling up space, *Appl. Phys. Lett.* **103**, 063509 (2013).
- [9] H. Zhou, S. Zhang, T. Zhu, Y. Tian, Y. Wang, and Y. Wang, Hybrid metasurfaces for perfect transmission and customized manipulation of sound across water–air interface, *Adv. Sci.* **10**, 2207181 (2023).
- [10] Zhandong Huang, Shengdong Zhao, Yiyuan Zhang, Zheren Cai, Zheng Li, Junfeng Xiao, Meng Su, Qiuquan Guo, Chuanzeng Zhang, Yaozong Pan, Xiaobing Cai, Yanlin Song, and Jun Yang, Tunable fluid-type metasurface for wide-angle and multifrequency water-air acoustic transmission, *Research* **2021**, 9757943 (2021).
- [11] R. Ghaffarivardavagh, J. Nikolajczyk, R. Glynn Holt, S. Anderson, and X. Zhang, Horn-like space-coiling metamaterials toward simultaneous phase and amplitude modulation, *Nat. Commun.* **9**, 1349 (2018).
- [12] Xudong Fan, Yifan Zhu, Zihao Su, Ning Li, Xiaolong Huang, Yang Kang, Can Li, Chunsheng Weng, Hui Zhang, Bin Liang, and Badreddine Assouar, Ultrabroadband and reconfigurable transmissive acoustic metascreen, *Adv. Funct. Mater.* **33**, 2300752 (2023).
- [13] J. Qian, J. Xia, H. Sun, Y. Wang, Y. Ge, S. Yuan, Y. Yang, X. Liu, and B. Zhang, Aperiodic metagratings for high-performance multifunctional acoustic lenses, *Adv. Mater. Technol.* **5**, 2000542 (2020).
- [14] L. Bai, H. Y. Dong, G. Y. Song, Q. Cheng, B. Huang, W. X. Jiang, and T. J. Cui, Impedance-matching wavefront-transformation lens based on acoustic metamaterials, *Adv. Mater. Technol.* **3**, 1800064 (2018).
- [15] X.-L. Tang, T.-X. Ma, and Y.-S. Wang, Topological rainbow trapping and acoustic energy amplification in two-dimensional gradient phononic crystals, *Appl. Phys. Lett.* **122**, 112201 (2023).
- [16] W. Gao, J. Xia, H. Sun, S. Yuan, Y. Ge, and X. Liu, Acoustic energy harvesting for low-frequency airborne sound based on compound Mie resonances, *Appl. Phys. Express* **12**, 044002 (2019).
- [17] N. Gao, Z. Zhang, J. Deng, X. Guo, B. Cheng, and H. Hou, Acoustic metamaterials for noise reduction: A review, *Adv. Mater. Technol.* **7**, 2100698 (2022).
- [18] N. Gao, J. Wu, K. Lu, and H. Zhong, Hybrid composite meta-porous structure for improving and broadening sound absorption, *Mech. Syst. Signal Process.* **154**, 107504 (2021).
- [19] X. Zhao, *et al.*, A scalable high-porosity wood for sound absorption and thermal insulation, *Nat. Sustainability* **6**, 306 (2023).
- [20] S. Kumar and H. P. Lee, Labyrinthine acoustic metastructures enabling broadband sound absorption and ventilation, *Appl. Phys. Lett.* **116**, 134103 (2020).
- [21] C. Liu, H. Wang, B. Liang, J. Cheng, and Y. Lai, Low-frequency and broadband muffler via cascaded labyrinthine metasurfaces, *Appl. Phys. Lett.* **120**, 231702 (2022).
- [22] Y. Zhu, K. Donda, S. Fan, L. Cao, and B. Assouar, Broadband ultra-thin acoustic metasurface absorber with coiled structure, *Appl. Phys. Express* **12**, 114002 (2019).
- [23] R. Dong, D. Mao, X. Wang, and Y. Li, Ultrabroadband acoustic ventilation barriers via hybrid-functional metasurfaces, *Phys. Rev. Appl.* **15**, 024044 (2021).
- [24] C. Gao, C. Hu, B. Hou, X. Zhang, S. Li, and W. Wen, Ventilation duct silencer design for broad low-frequency sound absorption, *Appl. Acoust.* **206**, 109324 (2023).
- [25] J. W. Jung, J. E. Kim, and J. W. Lee, Acoustic metamaterial panel for both fluid passage and broadband soundproofing in the audible frequency range, *Appl. Phys. Lett.* **112**, 041903 (2018).
- [26] X. Su and D. Banerjee, Extraordinary sound isolation using an ultrasparse array of degenerate anisotropic scatterers, *Phys. Rev. Appl.* **13**, 064047 (2020).
- [27] Y. Cheng, C. Zhou, B. G. Yuan, D. J. Wu, Q. Wei, and X. J. Liu, Ultra-sparse metasurface for high reflection of low-frequency sound based on artificial Mie resonances, *Nat. Mater.* **14**, 1013 (2015).
- [28] Jianping Xia, Ye-Yang Sun, Yi-Jun Guan, Yin Wang, Yu-Jing Lu, Hui-Gang Hu, Yong Ge, Hong-Xiang Sun, Shou-Qi Yuan, Yun Lai, and Xiao-Jun Liu, Broadband low-frequency sound absorption in open tunnels with deep sub-wavelength Mie resonators, *Front. Phys.* **10**, 1047892 (2022).



- [29] H. Q. Nguyen, Q. Wu, H. Chen, J. J. Chen, Y. K. Yu, S. Tracy, and G. L. Huang, A Fano-based acoustic metamaterial for ultra-broadband sound barriers, *Proc. R. Soc. A* **477**, [rspa.2021.0024](#) (2021).
- [30] H. Zhang, Y. Zhu, B. Liang, J. Yang, J. Yang, and J. Cheng, Omnidirectional ventilated acoustic barrier, *Appl. Phys. Lett.* **111**, 203502 (2017).
- [31] R. Ghaffarivardavagh, J. Nikolajczyk, S. Anderson, and X. Zhang, Ultra-open acoustic metamaterial silencer based on Fano-like interference, *Phys. Rev. B* **99**, 024302 (2019).
- [32] S. Gao, Y. Zhu, Z. Su, H. Zeng, and H. Zhang, Broadband ventilated sound insulation in a highly sparse acoustic meta-insulator array, *Phys. Rev. B* **106**, 184107 (2022).
- [33] Y.-F. Zhu, X.-Y. Zou, B. Liang, and J.-C. Cheng, Acoustic one-way open tunnel by using metasurface, *Appl. Phys. Lett.* **107**, 113501 (2015).
- [34] Y. Ge, H. Sun, S. Yuan, and Y. Lai, Switchable omnidirectional acoustic insulation through open window structures with ultrathin metasurfaces, *Phys. Rev. Mater.* **3**, 065203 (2019).
- [35] Y. Zhu, J. Hu, X. Fan, J. Yang, B. Liang, X. Zhu, and J. Cheng, Fine manipulation of sound via lossy metamaterials with independent and arbitrary reflection amplitude and phase, *Nat. Commun.* **9**, 1632 (2018).
- [36] See Supplemental Material <http://link.aps.org/supplemental/10.1103/PhysRevApplied.21.044045> for the calculation and the experimental evidence of the unit's transmission coefficient, the standard process of effective medium theory, the influence of the thermal viscous effect, a low-frequency sample, the impact of the incident sound source and the influence of the width of the ventilated gap.
- [37] L. Kinsler, *Fundamentals of Acoustics* (Wiley, New York, 1982).
- [38] V. Fokin, M. Ambati, C. Sun, and X. Zhang, Method for retrieving effective properties of locally resonant acoustic metamaterials, *Phys. Rev. B* **76**, 144302 (2007).
- [39] B. H. Song and J. S. Bolton, A transfer-matrix approach for estimating the characteristic impedance and wave numbers of limp and rigid porous materials, *J. Acoust. Soc. Am.* **107**, 1131 (2000).
- [40] H.-W. Dong, S.-D. Zhao, P. Wei, L. Cheng, Y.-S. Wang, and C. Zhang, Systematic design and realization of double-negative acoustic metamaterials by topology optimization, *Acta Mater.* **172**, 102 (2019).